Nanoscale

PAPER

Cite this: *Nanoscale*, 2019, **11**, 4073

Aggregation control of Ru and Ir nanoparticles by tunable aryl alkyl imidazolium ionic liquids†

Laura Schmolke,[a] Swantje Lerch,[b] Mark Bülow,[c] Marvin Siebels,[a] Alexa Schmitz,[a] Jörg Thomas,[d] Gerhard Dehm,[d] Christoph Held,[c] Thomas Strassner *[b] and Christoph Janiak *[a]

Metal-nanoparticles (M-NPs) were synthesized in a wet-chemical synthesis route in tunable aryl alkyl ionic liquids (TAAILs) based on the 1-aryl-3-alkyl-substituted imidazolium motif from $Ru_3(CO)_{12}$ and $Ir_4(CO)_{12}$ by microwave-heating induced thermal decomposition. The size and size dispersion of the NPs were determined by transmission electron microscopy (TEM) to an average diameter of 2.2(±0.1) to 3.9 (±0.3) nm for Ru-NPs and to an average diameter of 1.4(±0.1) to 2.4(±0.1) nm for Ir-NPs. The TAAILs used contain the same bis(trifluoromethylsulfonyl)imide anion but differ in the substituents on the 1-aryl ring, *e.g.* 2-methyl-, 4-methoxy- and 2,4-dimethyl groups and in the 3-alkyl chain lengths (C_4H_9, C_5H_{11}, C_8H_{17}, C_9H_{19}, $C_{11}H_{23}$). All used TAAILs are suitable for the stabilization of Ru- and Ir-NPs over months in the IL dispersion. Different from all other investigations on M-NP/IL systems which we are aware of the particle separation properties of the TAAILs vary strongly as a function of the aryl substituent. Good NP separation can be achieved with the 4-methoxyphenyl- and 2,4-dimethylphenyl-substituted ILs, irrespective of the 3-alkyl chain lengths. Significant aggregation can be observed for 2-methylphenyl-substituted ILs. The good NP separation can be correlated with a negative electrostatic potential at the 4-methoxyphenyl or 4-methylphenyl substituent that is in the *para*-position of the aryl ring, whereas the 2-(*ortho*-) methylphenyl group assumes no negative potential. ε-ePC-SAFT calculations were used to validate that the interactions between ILs and the washing agents (required for TEM analyses) do not cause the observed aggregation/separation behaviour of the M-NPs. Ru-NPs were investigated as catalysts for the solvent-free hydrogenation of benzene to cyclohexane under mild conditions (70 °C, 10 bar) with activities up to 760 (mol cyclohexane) (mol Ru)$^{-1}$ h^{-1} and over 95% conversion in ten consecutive runs for Ru-NPs. No significant loss of catalytic activity could be observed.

Received 20th December 2018,
Accepted 8th February 2019

DOI: 10.1039/c8nr10286d

rsc.li/nanoscale

Introduction

Transition metal nanoparticles (M-NPs) attract wide interest due to their various applications in medicine,[1,2] optics,[3,4] electronics[5] and luminescence.[6] The large surface area resulting from the small size of M-NPs supplies a variety of opportunities in the catalysis.[7–10] Ruthenium nanoparticles (Ru-NPs) are attractive catalysts because of their lower economical price compared to other noble metals such as palladium or platinum. The selectivity of Ru-NP catalysts for the hydrogenation of C=C carbon double bonds in alkenes or arenes[11–13] allows an application in hydrogenation of benzene or cyclohexene to cyclohexane.[14–17] Especially small NPs are interesting for the catalysis. However, the small size of M-NPs results in an agglomeration and aggregation in the process of Ostwald-ripening.[18,19] To avoid agglomeration the M-NPs have to be stabilized sterically or electrostatically.[20] The stabilization of M-NPs by capping ligands, surfactants or polymers results in a change of the surface properties with remark to applications in catalysis.[21] Alternatively, ionic liquids (ILs) are utilized as stabilizing reagents and as solvents in the synthesis of NPs.[22–24] Electrostatic and steric interactions play a role in the stabilization of M-NPs by ILs without any change in surface

[a]*Institut für Anorganische Chemie und Strukturchemie, Heinrich-Heine-Universität Düsseldorf, 40204 Düsseldorf, Germany. Fax: +49-211-81-12287; Tel: +49-211-81-12286; E-mail: janiak@uni-duesseldorf.de*
[b]*Professur für Physikalische Organische Chemie, Technische Universität Dresden, 01062 Dresden, Germany. Fax: +49-351-463-39679; Tel: +49-351-463-38571; E-mail: thomas.strassner@chemie.tu-dresden.de*
[c]*Laboratory of Thermodynamics, Technische Universität Dortmund, Emil-Figge-Str 70, 44227 Dortmund, Germany. Fax: +49-231-755-2572; Tel: +49-231-755-2086; E-mail: Christoph.Held@tu-dortmund.de*
[d]*Department Structure and Nano-/Micromechanics of Materials, Max-Planck-Institut für Eisenforschung GmbH, 40237 Düsseldorf, Germany*

† Electronic supplementary information (ESI) available: TAAIL synthesis and analysis, IL viscosity data, IR-spectra, TEM images with particle size histograms, SAEDs, details of ε-ePC-SAFT calculations, surface atom calculations and additional activity-time plots for catalysis. See DOI: 10.1039/c8nr10286d

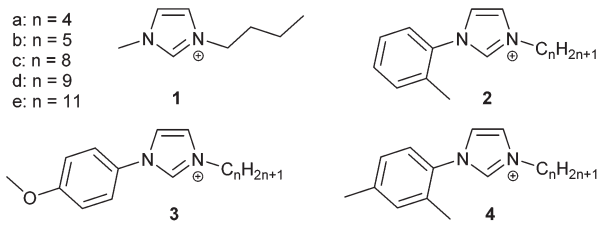

Fig. 1 Structure of the 1,3-disubstituted imidazolium IL cation (**1**) and the different TAAIL cations (**2–4**) with different aryl substitutions.

properties.[20,25–27] In addition, their high ionic charge, polarity and dielectric constant turn the ILs into an ideal media for microwave reactions and for the stabilization of M-NPs.[28–30] The stabilization of M-NPs in non-functionalized ILs such as 1-butyl-3-methylimidazolium bis(trifluoromethylsulfonyl)imide ([BMIm]NTf_2) appears to be primarily based on the IL-anions, which probably form the immediate layer around the NP.[31–33]

TAAILs are a new class of ILs bearing a phenyl ring on the N1-atom of the imidazolium ring and an alkyl chain at the N3 position (Fig. 1).[34] In comparison with all-alkyl imidazolium ILs, the aromatic moiety introduces a sp^2 hybridized carbon atom bound to the nitrogen leading to altered physical properties such as a high thermal stability, and additional steric as well as electronic effects.[35] This molecular structure gives rise to excellent solubility of metal salts which can be used for metal extraction or catalysis.[36,37]

Synthesis of Ru-NPs is possible by decomposition of zerovalent compounds, such as $Ru_3(CO)_{12}$[21,38,39] or [Ru(cyclooctadiene)(cyclooctatetraene)][40–42] without the need of a reducing agent under microwave irradiation. The carbonyl (CO) side product is removed through the gas phase and does not remain in the M-NP/IL dispersion. Contamination from by- or decomposition products, which are otherwise generated during the M-NP synthesis are therefore significantly reduced.[32,39,43,44]

Through our past work on M-NP/IL systems[15–17,20,21,31–33] we have not come across, and to the best of our knowledge we are not aware of ILs which can influence or control the separation or aggregation of the synthesized M-NPs.

Here, we report on TAAILs as a new group of ILs for the stabilization and as a synthesis media for M-NPs. In this work different aggregation effects of the TAAILs became evident which we investigated as a function of the aryl substituent by employing 4-methoxyphenyl-, 2-methylphenyl- and 2,4-dimethylphenyl-substituted TAAILs. Hence, the aim of this study is to elucidate the controlling effects of the ionic liquids for the metal nanoparticle separation or aggregation. Further, the influence of separated or aggregated Ru-NPs and their recyclable catalytic properties were tested towards the hydrogenation of benzene.[16,45]

Experimental section

Coulometric Karl Fischer titration (Table S2†) was performed with an ECH/Analytik Jena AQUA 40.00 Karl Fischer titrator. The measurements were done with the headspace module with dried sample container and crimp caps (∅ = 20 mm, with PTFE septum). The sample containers and crimp caps were dried at 70 °C for 2 days. The measurements were done at an oven temperature of 170 °C.

Thermogravimetric analysis (TGA) (Table S1 and Fig. S1–S2 in the ESI†) was carried out with a Netzsch TG 209 F3 Tarsus, equipped with Al-crucible using a heating rate of 5 K min^{-1} under inert atmosphere (N_2).

All ion chromatographic measurements (IC) (Table S2 and Fig. S3–S12 in the ESI†) were carried out using a Dionex ICS 1100 instrument with suppressed conductivity detection. The suppressor (AERS 500, Dionex) was regenerated with an external water module. The system was equipped with the analytical column IonPac AS 22 from Dionex (4 × 250 mm) with the corresponding guard column AG 22 (4 × 50 mm), respectively. The instrument was controlled by Chromeleon® software (version 7.1.0.898). The injection volume was 25 μL. The standard eluent used was a 4.5 mmol L^{-1} Na_2CO_3 + 1.0 mmol L^{-1} $NaHCO_3$ mixture with an addition of 30 vol% acetonitrile (ACN).

Viscosities were measured using a Brookfield DV2T viscometer. 0.5 mL of the corresponding TAAIL was dried in high vacuum to a water content below 100 ppm and was then measured from 20 °C to 80 °C in 5 K steps (see Tables S3–S6 in the ESI†).

IR-spectra were recorded on a Bruker Tensor 37 IR with ATR unit in the range of 4000–600 cm^{-1}.

The TEM imaging was performed on a Philips CM20 electron microscopy operated at 200 kV accelerating voltage. Samples were prepared using 200 μm carbon-coated copper grids. 0.05 mL of the NP/IL dispersion was dissolved in 0.5 mL ACN and one drop of the diluted dispersion was placed on the grid. After 30 minutes, the grid was washed with 3 mL ACN and dried in a nitrogen stream. The size distribution was determined manually or with the aid of a digital micrograph from at least 500 individual particles at different position on the TEM grid with the same magnifications.

Examples of selected area electron diffraction (SAED) patterns (Fig. S43–S50 in the ESI†) have been recorded with a Philips CM20 TEM, operated at 200 kV accelerating voltage. For each acquisition, a sample region with a significant amount of material was placed inside the aperture. The objected was illuminated with wide-spread parallel beam obtaining focused diffraction patterns. The diffraction images were calibrated with Debye–Scherrer patterns recorded from a gold reference sample (S106, Plano GmbH, Wetzlar, Germany).

Powder X-ray diffractograms, PXRDs were measured at ambient temperature on a Bruker D2-Phaser using a flat sample holder and Cu-Kα radiation (λ = 1.54182 Å, 35 kV) (Fig. S55 in the ESI†).

Conversion of benzene to cyclohexane was determined by gas chromatography (GC) (PerkinElmer 8500 HSB 6, equipped with a DB-5 film capillary column, 60 m × 0.32 mm, film thickness 25 μm, oven temperature 33 °C, N_2 carrier flow 105 L min^{-1}, 180 °C injection temperature, 75 °C auxiliary gas (Aux) temperature and a flame ionization detector (FID), 250 °C detector temperature).

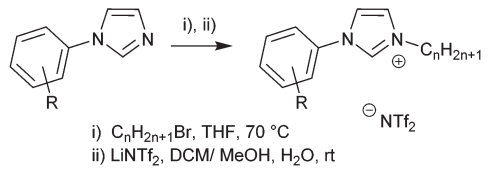

Scheme 1 The general synthesis of TAAILs with different aryl substitutions and chain lengths.

The electrostatic surface potentials (ESP) of the different IL cations were obtained based on the ground state geometry calculated with Gaussian 16 [46] at the B3LYP/6-311++g(d,p) level of theory.[47–50] All structures were verified as minima by vibrational frequency analysis and the absence of negative eigenvalues. Results have been visualized using GaussView6.[51]

Synthesis of the TAAILs

The synthesis of the TAAILs was a two step synthesis (Scheme 1) starting from substituted aryl imidazoles. The first step was the alkylation of the aryl imidazoles by bromoalkanes to yield the IL-cations with bromide anions. In the second step, the anion (bromide) was exchanged with $LiNTf_2$. The detailed synthesis and characterization of the TAAILs is reported in the ESI.†

M-NP synthesis

Decomposition by microwave heating was carried out under a nitrogen atmosphere. The metal carbonyls were dissolved/suspended (for about 12 h) at room temperature in the TAAILs. Mass of the metal carbonyls was set for 0.5 or 1.0 wt% M-NP in IL dispersion. The mixture was placed in a microwave (CEM, Discover) and irradiated for 10 min at a power of 50 W to an indicated temperature of 230 °C.

Hydrogenation reactions

All catalytic processes were done in a stainless-steel autoclave with glass inlay. In preparation for the hydrogenation reactions, the M-NPs were purified from the excess ILs by washing with 6 mL dry ACN. The purification resulted in a black powder. At the same time, TEM images of these washed M-NPs have shown that the primary particles stay separated, presumably due to a remaining immediately surrounding IL-layer (Fig. S54 in the ESI†). The catalyst and the substrate (benzene) were loaded in the autoclave and purged three times with H_2. The stirring rate was 800 rpm and the heating temperature was 70 °C. After 30 minutes, the autoclave was charged with 10 bars of H_2. The reaction was stopped at maximal conversion and the products were analyzed by headspace GC. The hydrogenation runs were repeated several times.

Results and discussion

The general synthesis of TAAILs is shown in Scheme 1 and the structures of the employed TAAIL cations used are depicted in Fig. 1. The corresponding ILs **2a** to **4e** can be obtained in large gram scale and the synthesis route tolerates a variety of aryl substitutions as well as alkyl chains (see details in ESI†).

The ILs were characterized by NMR, ion chromatography, Karl Fischer titration and elemental analysis (details are given in the ESI†). The anion purity was determined by ion chromatography to be above 98.8 wt% (Table S2 and Fig. S3–S12 in the ESI†).[52] Thermogravimetric analysis (TGA) revealed that all TAAILs decompose at temperatures higher than 340 °C and are therefore suitable for microwave irradiation at 230 °C (Table S1 and Fig. S1 in the ESI†).

The synthesis of M-NPs from metal carbonyls in ILs is well known.[15,16,39,43] Ruthenium or iridium carbonyl ($Ru_3(CO)_{12}$ or $Ir_4(CO)_{12}$) were suspended in the IL. Precursor decomposition by microwave irradiation in ILs was achieved within 10 minutes using a power of 50 W to give a temperature of about 230 °C in the reaction mixture (Scheme 2). A black NP dispersion was reproducibly obtained by repeated decompositions of the precursors in the TAAILs.

Small M-NPs with an average size below 4 nm and small size dispersions of mostly ±0.1–0.3 nm were readily obtained, according to TEM analysis (Table 1). The small particle size is explained by the microwave assisted synthesis. Rapid heating

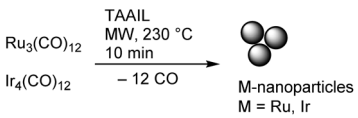

Scheme 2 Synthesis scheme of ruthenium- and iridium-nanoparticles from $Ru_3(CO)_{12}$ or $Ir_4(CO)_{12}$ by microwave (MW) assisted thermal decomposition in TAAILs.

Table 1 M-NP size determination in TAAILs[a]

TAAIL	Identity[b]	TEM Ø[c,d], (nm)
1-Butyl-3-methyl imidazolium IL		
$[BMIm]NTf_2$ (**1**)	Ru	2.7 ± 0.1
	Ir	1.7 ± 0.1
2-Methylphenyl-substituted TAAIL		
$[Ph_{2\text{-}Me}\_Im\_C4]NTf_2$ (**2a**)	Ru	3.9 ± 0.1
$[Ph_{2\text{-}Me}\_Im\_C5]NTf_2$ (**2b**)	Ru[e]	3.5 ± 0.3
	Ir	2.3 ± 0.1
$[Ph_{2\text{-}Me}\_Im\_C9]NTf_2$ (**2d**)	Ir[e]	1.4 ± 0.1
$[Ph_{2\text{-}Me}\_Im\_C11]NTf_2$ (**2e**)	Ir	1.8 ± 0.1
4-Methoxy-substituted TAAIL		
$[Ph_{4\text{-}OMe}\_Im\_C5]NTf_2$ (**3b**)	Ru	3.9 ± 0.3
$[Ph_{4\text{-}OMe}\_Im\_C8]NTf_2$ (**3c**)	Ru[e]	2.2 ± 0.1
$[Ph_{4\text{-}OMe}\_Im\_C11]NTf_2$ (**3e**)	Ir	1.5 ± 0.1
2,4-Dimethylphenyl-substituted TAAIL		
$[Ph_{2,4\text{-}Me}\_Im\_C5]NTf_2$ (**4b**)	Ru	3.3 ± 0.1
	Ir	1.5 ± 0.1
$[Ph_{2,4\text{-}Me}\_Im\_C9]NTf_2$ (**4d**)	Ir	1.6 ± 0.1
$[Ph_{2,4\text{-}Me}\_Im\_C11]NTf_2$ (**4e**)	Ir[e]	1.5 ± 0.1

[a] 0.5/1.0 wt% M-NP/TAAIL dispersions obtained by microwave-assisted heating for 10 min at 230 °C. [b] The identity of the NPs was determined by ATR-IR and SAED. [c] Average diameter (Ø). [d] See Experimental section for TEM measurement conditions; at least 500 particles were used for the size analysis. [e] Amorphous.

to above 230 °C within ~2 min by microwave irradiation leads to a rapid decomposition of the carbonyl precursors, hence a high rate for the formation of the nucleation sites. The large number of seeds thus formed, can only grow until the available starting material has been used up. Because ILs show a high dissipation factor (tan δ) for the conversion of microwave energy into heat[29,53] this leads to localized superheating. As soon as metal particles have formed, they will also absorb the microwave radiation, thereby creating 'hot spots' where the temperature will be even higher than the average temperature reading for the whole sample. Further, the small size is evidence that the growing NPs are effectively stabilized by the IL already in the early growth stages.[54] We also note that the solid metal carbonyls were and had to be finely dispersed in the IL by stirring for several hours. Upon immediate microwave irradiation of little-dispersed metal carbonyl in IL hot spots are formed at the solid particles which melt the glass of the vial.

The crystalline parts of the M-NPs were phase pure face centered cubic (fcc) Ru or fcc Ir metal as seen from selected area electron diffraction (SAED) (Fig. S43–S50 in the ESI†). Each sample was analyzed on a large scale and TEM images were taken from different positions on the grid to ensure the representative nature of the depicted aggregation. Complete decomposition of the metal carbonyl was ascertained by the disappearance of the characteristic carbonyl stretches between 2057–1982 cm^{-1} by attenuated total reflection infrared spectroscopy (ATR-IR) (Fig. 2 and Fig. S13–S26 in the ESI†).

Ru-NPs in TAAILs

Fig. 3 shows representative TEM pictures of the Ru-NPs obtained from the decomposition of $Ru_3(CO)_{12}$ in different TAAILs. The average particle size is between 2.2 and 3.9 nm with size distributions as standard deviation (σ) usually between ±0.1–0.3 nm (Table 1). The 2-methylphenyl-substituted TAAILs **2a** and **2b** lead to an aggregation of the primary NPs.

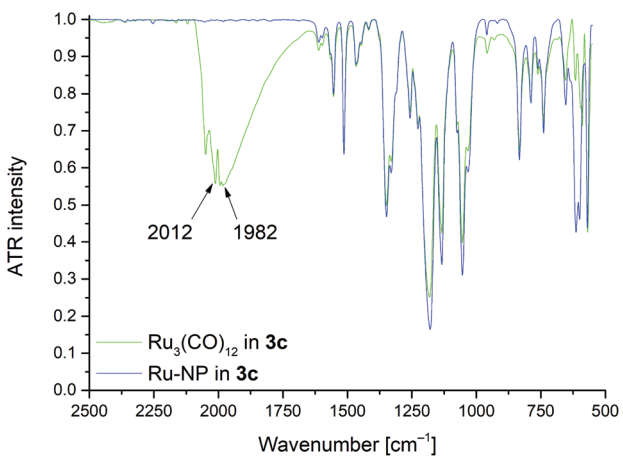

Fig. 2 ATR-IR spectra of $Ru_3(CO)_{12}$/TAAIL **3c** dispersion (green) with the metal-bound carbonyl stretches at 2012 cm^{-1} and 1982 cm^{-1} for the terminal and bridging CO ligands and the resulting Ru-NP/TAAIL **3c** dispersion (blue) after microwave irradiation. See Fig. S13–S16 in ESI† for the analogous ATR-IR spectra of $Ir_4(CO)_{12}$/TAAIL.

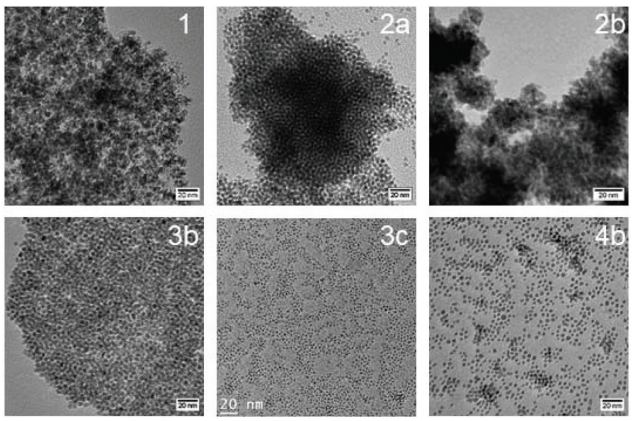

Fig. 3 TEM pictures of Ru-NPs from $Ru_3(CO)_{12}$ in different TAAILs at uniform magnifications with scale bars of 20 nm: [BMIm]NTf_2 (**1**) ([$Ph_{2\text{-}Me}$_Im_C4]NTf_2 (**2a**), [$Ph_{2\text{-}Me}$_Im_C5]NTf_2 (**2b**), [$Ph_{4\text{-}OMe}$_Im_C5]NTf_2 (**3b**), [$Ph_{4\text{-}OMe}$_Im_C8]NTf_2 (**3c**) and [$Ph_{2,4\text{-}Me}$_Im_C5]NTf_2 (**4b**). See the Fig. S27–S40 in the ESI† for further TEM images and histograms of the particle size distributions.

The primary Ru-NPs which were obtained in the 4-methoxyphenyl- or 2,4-dimethylphenyl-substituted TAAILs **3b**, **3c** and **4b** were well separated. The Ru-NPs in 3-pentyl-1-(4-methoxyphenyl)-1*H*-imidazolium IL (**3b**) form a close-packed array when brought onto the TEM grid (Fig. 3). Each NP is surrounded mostly by six, occasionally also five or seven other NPs.

To determine whether TAAILs provide a better separation compared to "common" 1,3-dialkylimidazolium ILs, Ru-NPs were synthesized in [BMIm]NTf_2 (**1**) following the same synthesis route. The NPs are clearly more aggregated than the NPs in the TAAILs **3b**, **3c** and **4b**.

Ir-NP in TAAILs

Fig. 4 shows representative TEM pictures of the iridium-nanoparticles (Ir-NPs) obtained from the decomposition of $Ir_4(CO)_{12}$ in different TAAILs. The average particle size is between 1.3 and 2.4 nm with size distributions as standard deviation (σ) usually between ±0.1–0.2 nm (Table 1). The Ir-NPs are consistently slightly smaller than the Ru-NPs (Table 1). This can be explained by either a faster decomposition rate for $Ir_4(CO)_{12}$ over $Ru_3(CO)_{12}$, hence more rapid nucleation for Ir over Ru, or a slower growth rate for Ir over Ru. Thermogravimetry shows an earlier onset for $Ru_3(CO)_{12}$ than $Ir_4(CO)_{12}$ decomposition (Fig. S2†). Yet, this difference in thermodynamic stability does not reflect the reaction kinetics for decomposition, cluster nucleation and growth when the reaction energy is available. With a limited amount of precursor, a faster nucleation rate will lead to smaller particles. The same is true for slower nucleation together with a much slower growth rate.

The 2-methylphenyl-substituted TAAILs **2b** and **2e** lead again to an aggregation of the primary Ir-NPs. The degree of aggregation in the 2-methylphenyl-TAAIL **2d** and in the 4-methoxyphenyl-TAAIL **3e** is less, albeit the NPs arranged in partially ordered two-dimensional layers, as seen before for

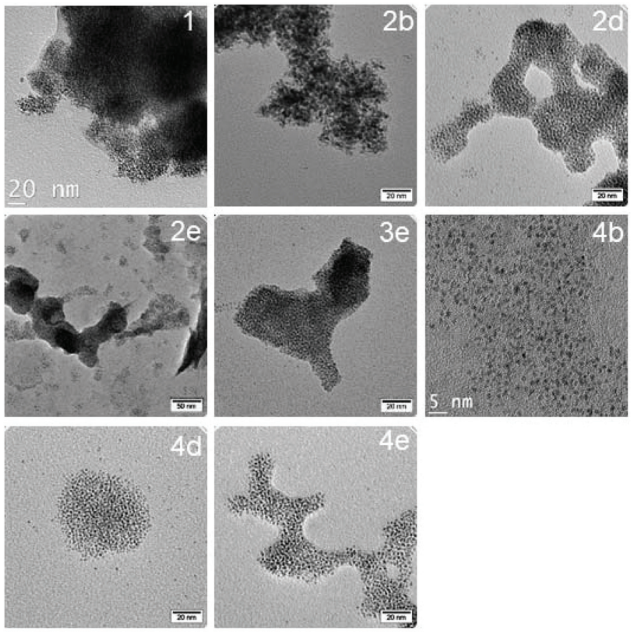

Fig. 4 TEM pictures of Ir-NP from $Ir_4(CO)_{12}$ in different TAAILs at uniform magnifications with scale bars of 20 nm, except **4b**: [BMIm]NTf_2 (**1**), ([$Ph_{2\text{-}Me}$_Im_C5]NTf_2 (**2b**), [$Ph_{2\text{-}Me}$_Im_C9]NTf_2 (**2d**), [$Ph_{2\text{-}Me}$_Im_C11]NTf_2 (**2e**), [$Ph_{4\text{-}OMe}$_Im_C11]NTf_2 (**3e**), [$Ph_{2,4\text{-}Me}$_Im_C5]NTf_2 (**4b**), [$Ph_{2,4\text{-}Me}$_Im_C9]NTf_2 (**4d**), and [$Ph_{2,4\text{-}Me}$_Im_C11]NTf_2 (**4e**). See the Fig. S27–S40 in the ESI† for further TEM images and histograms of the particle size distributions.

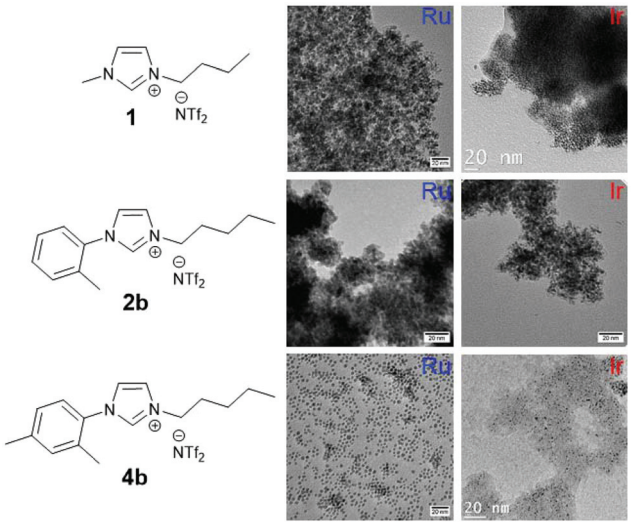

Fig. 5 Exemplary correlation of the aryl substitution of the TAAIL cation (left) and different aggregation pattern from TEM images of Ru-NP (middle) and Ir-NP (right) for 1-butyl-3-methyl imidazolium (**1**), 2-methyl- (*e.g.* **2b**) and 2,4-dimethyl (*e.g.* **4b**) substituted aryl rings.

Ru-NPs with the IL **3b**. Only the primary Ir-NPs, which were obtained in the 2,4-dimethylphenyl-substituted TAAILs **4b**, **4d** and **4e**, were rather well separated (Fig. 4). Ir-NPs which were synthesized in 1-butyl-3-methylimidazolium bis(trifluoromethylsulfonyl)imide (**1**) were again clearly more aggregated than the NPs in the TAAILs **2d**, **4b**, **4d** and **4e**.

In view of the very small size range of both the Ru- and Ir-NPs, respectively, a possible influence of the 3-alkyl chain length of the imidazolium cation in the TAAIL on the particles size is not evident (Fig. S41 in the ESI†). In the literature, longer alkyl chain lengths are reported to cause either an increase[55,56] or decrease[57] in NP size. For Ru-NPs, the interaction energy of imidazolium cations with long alkyl chain lengths ($C > 6$) was found to be higher than the interaction energy with short alkyl chain lengths ($C = 4$).[58] Other sources state a non-existing influence between alkyl chain length and particle size.[17]

Analysis of NP aggregation in TAAILs

All used TAAILs are suitable for the microwave-induced synthesis of Ru- and Ir-NPs, but they induce different separation or aggregation effects of the NPs.

In summary, good NP segregation was largely observed for the 4-methoxyphenyl-substituted TAAILs **3** (for Ru) and for the 2,4-dimethylphenyl-substituted TAAILs **4** (for both Ru and Ir, Fig. 5). Whereas for 2-methylphenyl-substituted TAAILs **2** (for both Ru and Ir, Fig. 5), a significant aggregation was found.

Especially, the strong influence of the 4-methylphenyl substituent on the aryl ring, which prevents NP aggregation, is surprising. We therefore attempted to evaluate the substitution effect by calculating the electrostatic surface potentials (ESP). Fig. 6 shows the ESP plots of the imidazolium cations of the ILs **2b**, **3b** and **4b**. The calculations suggest that both the oxygen atom of the 4-methoxy (**3b**) and the 4-methyl (**4b**) group assume a negative electrostatic potential, which seems to be crucial for low NP aggregation. The 2-methylphenyl-substituent in the TAAILs **2** and **4** has no negative electrostatic potential on the *ortho* position. We note that the highly negative electrostatic potential at the terminal methyl group of the alkyl chain does not seem to contribute to the segregation or aggregation effect of the TAAILs.

We also investigated the viscosity and density of the TAAILs (Table 2 and Tables S3–S6 in the ESI†). The viscosity measurements indicate that all TAAILs have an intermediate viscosity

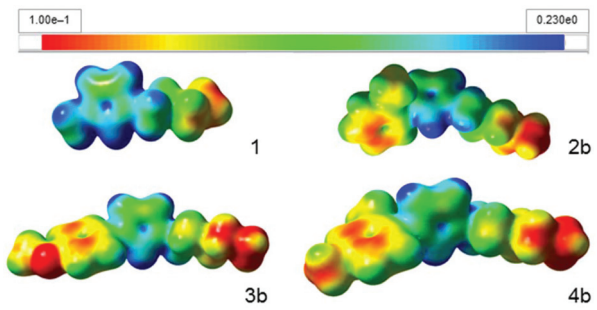

Fig. 6 Electrostatic surface potential plots of butyl-methylimidazolium **1** and the three different substituted aryl rings in the TAAILs cations, exemplified by **2b** (for 2-methyl), **3b** (for 4-methoxy) and **4b** (for 2,4-dimethyl).

Table 2 Viscosity and densities of different TAAILs measured at 20 °C

TAAIL	Viscosity (cP)[a]	Density (g cm^{-3})
[$Ph_{2\text{-}Me}$_Im_C4]NTf_2 (**2a**)	419 ± 9	—
[$Ph_{2\text{-}Me}$_Im_C5]NTf_2 (**2b**)	437 ± 9	1.396
[$Ph_{4\text{-}OMe}$_Im_C5]NTf_2 (**3b**)	591 ± 9	1.399
[$Ph_{2,4\text{-}Me}$_Im_C5]NTf_2 (**4b**)	690 ± 9	1.349

[a] Measured at room temperature.

between 419 and 690 cP. As viscosity decreases in a logarithmic function with temperature, these differences become almost negligible at the reaction temperature of 230 °C. Therefore, there is no effect of the viscosity on the formation of the M-NPs. Also, the viscosity range of the ILs at 20 °C between 419 to 690 cP is not large enough to rationalize the observed aggregation differences. The differences of the densities of the TAAILs are also too small to be taken as the basis of any change in the aggregation of the NPs.

NP–NP aggregation is not mediated by IL–solvent interactions

It might be possible that the aggregation of the NPs is an artefact of the TEM grid preparation. The TEM samples have been prepared by diluting 0.05 mL of the NP/IL dispersion with 0.5 mL ACN. One drop of this dispersion was placed on the TEM grid and dried in a nitrogen stream. After 30 minutes, the grid was carefully washed with 3 mL ACN and dried again. The interactions of the ILs with the solvents upon washing might hinder or enhance the self-interactions of the M-NPs; this solvent-mediated effect might explain the aggregation/separation behaviour of the M-NPs observed in the TEM. Thus, to rule out a possible artefact of the TEM images through the washing procedure of the sample preparation, a possible correlation between the solubility of the TAAILs in the washing agents (*i.e.* the solvents) and the aggregation of the M-NPs was investigated. The four TAAILs **2b**, **3b**, **3e** and **4b** have been considered as they cause different M-NP aggregation effects.

Therefore, an IL solubility screening in different solvents (water, *n*-hexane, and in the two washing agents dichloromethane (DCM) and ACN was performed by means of thermodynamic model predictions. In this work, ε-ePC-SAFT equation of state was used for that purpose. ε-ePC-SAFT is a new model for systems containing ILs. It was successfully used for the modelling of solubility in systems containing ILs[59] and is an extension to the original ePC-SAFT.[60–63] For further information on the method and its application, see section 8 in the ESI.† To exclude solvent-mediated interactions of the washing agents on the aggregation/separation behaviour of the M-NPs, qualitative statement on the solubility predictions with ε-ePC-SAFT is summarized in Table 3.

All mixtures of ACN + IL and DCM + IL were predicted to be completely miscible. Thus, this phase behaviour is independent of the kind of IL; this is a first hint for the fact that solvent-IL interactions are not responsible for aggregation effects. The modelling was performed without using binary interaction parameters and thus, the predicted miscibility had to be additionally verified two-fold. First, 1 : 1 (v : v) mixtures of ACN + IL and DCM + IL were prepared, and a single stable liquid phase was observed for every mixture, *i.e.* phase separation did not occur within a period of one week. Second, to further confirm the predictions, the solubility of the ILs in water and in *n*-hexane was predicted with ε-ePC-SAFT. The calculated numerical results can be found in Table S12 in the ESI.† To summarize these findings, inhomogeneity was predicted with ε-ePC-SAFT for all mixtures water + IL, and for all mixtures *n*-hexane + IL. The only exception was the mixture *n*-hexane + IL **4b**, for which ε-ePC-SAFT did not predict the coexistence of two different phases; this result has a minor impact on the general findings. As to be expected, the solubility of the considered ILs in water decrease with increasing hydrophobic tail, and *vice versa* for the IL solubility in *n*-hexane. To make the statement more quantitative, the exact values of the activity coefficients were investigated for IL–ACN and IL–DCM mixtures. This was verified by a comparison of the activity coefficients of all ILs under investigation in the mixtures. Activity coefficients lower than unity indicate that the IL is attracted to the solvent resulting in homogenous mixtures. These ε-ePC-SAFT predicted results are shown in Fig. 7. It can be observed that all activity coefficients are significantly lower than unity (0.05–0.25) and comparable in an absolute scale. The interactions between IL–ACN are very similar to the interaction IL–DCM, suggesting that both solvents have a comparable influence on the grid preparation.

However, there are huge differences in activity coefficients within a homologous series. For increasing chain length the activity coefficients of the ILs decrease significantly, which indicates the strong dependency of the cation chain length on IL–solvent interactions. However, a dependency between aggre-

Table 3 Overview on the miscibility of different solvents with the investigated ILs

Solvent Ionic liquid	Water[a]	*n*-Hexane[a]	ACN[b]	DCM[b]
2b	LLE	LLE	Completely miscible*	Completely miscible*
3b	LLE	LLE	Completely miscible*	Completely miscible*
3d	LLE	LLE	Completely miscible*	Completely miscible*
4b	LLE	Completely miscible	Completely miscible*	Completely miscible*

[a] LLE = liquid–liquid equilibria. [b] Calculated miscibility is in agreement with IL-solvent mixing experiments which show no phase separation over one week.

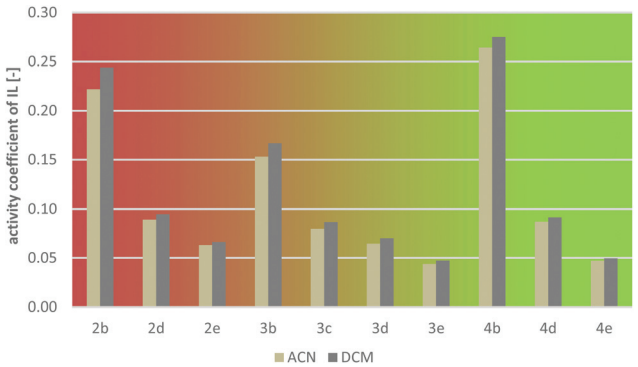

Fig. 7 Activity coefficients of the investigated ILs in the washing agents ACN or DCM predicted with ε-ePC-SAFT using the parameters listed in Table S8.† Conditions: p = 1 bar, T = 298.15 K, x_{IL} = 0.5 mol mol^{-1}. High NP aggregation on the left hand side (orange) and good NP separation on the right side (green).

gation and alkyl chain length of the cation was not observed experimentally.

Additionally, Fig. 7 allows comparing IL–solvent interactions for ILs that cause very different experimental aggregation behaviour. The four TAAILs **2b**, **3b**, **3e** and **4b** were classified into causing NP separation (**3b**, **3e**, **4b**) and NP aggregation (**2b**). It can be seen in Fig. 7 that the activity coefficients of **2b** and of **4b** are practically identical. Based on these ε-ePC-SAFT results, it can be concluded that IL–solvent interactions do not cause NP–NP aggregation. Thus, it is confirmed that the use of ACN or DCM as washing agents did not cause the observed aggregation effects. An artefact-like effect on the aggregation through differences in the IL–solvent interaction can thus be excluded.

Hydrogenation of benzene with Ru-NP produced in TAAILs

Ru-NPs with different degree of aggregation in the TAAILs **2b** (agglomerated) and **4b** (separated) (Fig. 3) were tested for their catalytic activity in the hydrogenation of benzene to cyclohexane (Scheme 3).

The hydrogenation of benzene to cyclohexane has been studied extensively[64–67] and is of great interest in the petroleum industry and for the industrial production of cyclohexane. In Diesel fuel the aromatic content needs to be removed by hydrogenation to fulfill environmental regulations.[68,69] Cyclohexane is important for the synthesis of fine chemicals[70] and is used, for example, as a precursor for the production of nylon-6 and nylon-66.[71]

Freshly synthesized Ru-NPs were used in a Büchi high-pressure, stainless-steel autoclave under IL- and organic solvent-free conditions. The autoclave was charged with the Ru-NPs (4 mg) and the substrate (0.9 g). The autoclave was purged with H_2 at least three times and was heated to 70 °C. After reaching the reaction temperature, the autoclave was pressurized with 10 bar of H_2. The reaction was stopped at maximal conversion and the product was analyzed by headspace gas chromatography. The hydrogenation runs were repeated with catalyst recycling by removing the volatile product (and possibly remaining substrate) through the gas phase in vacuum and charging the autoclave with fresh substrate under inert conditions. At the end, the Ru-NPs were checked by TEM, SAED and PXRD for differences to the pre-catalysis state (Fig. S54 and S55 in the ESI†). Also the TOF values were calculated for 95% conversion because the reaction rate decreases with the decrease in benzene substrate concentration (Fig. 8, Table 4).

It could be observed that the activity of the Ru/**4b** catalyst increased up to the eighth run to reach a TOF of 760 h^{-1}. The conversion was nearly quantitative for all hydrogenation runs. The increase in activity could result from surface cleaning of adsorbed and deactivating solvent, carbon or oxygen species, or an initially present CO cover of active sites, which has to be removed first. After ten runs the Ru-NPs grew from 3 to 4 nm and began to agglomerate (Fig. S54 in the ESI†), even if there was no significant loss of catalytic activity. Also, after ten runs, the nanoparticles had assumed a slime-like texture, which did not even solidify with several washing steps.

Even before catalysis, the crystallinity of the Ru-NPs was very low, as evidenced by the broad reflection between 40–50° 2theta (Fig. S55, ESI†). For an effective catalysis, the amount of Ru-NPs was kept as small as possible. These small amounts of Ru-NPs, which were subsequently available for PXRD analysis, did not allow obtaining a meaningful diffraction diagram (Fig. S55, ESI†). Alternatively, SAEDs were measured on TEM images of the nanoparticles (Fig. S54, ESI†), showing the fcc phase for the Ru-NPs before and after catalysis (Fig. 9).

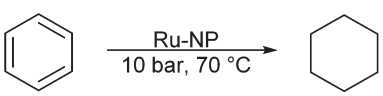

Scheme 3 Hydrogenation of benzene to cyclohexane with Ru-NPs produced in TAAILs.

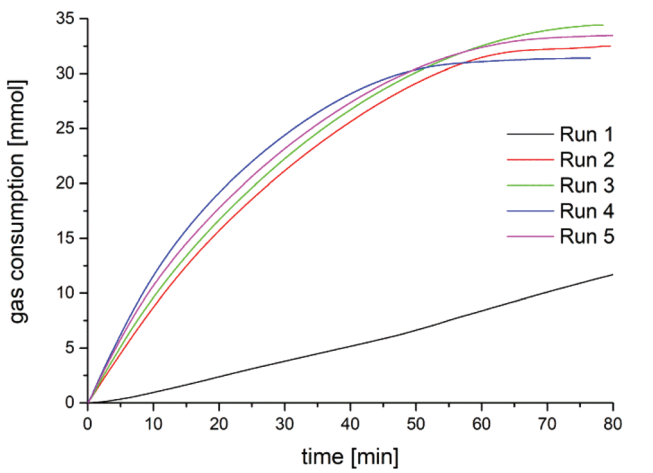

Fig. 8 H_2-uptake over time for the hydrogenation of benzene (0.91 g, 1.0 mL, 11.7 mmol) with Ru/**4b** (5.1 mg, 5.05 × 10^{-2} mmol), 70 °C and 10 bar H_2. For clarity, the runs 6–10 are given in Fig. S52 in the in the ESI.†

Table 4 Hydrogenation of benzene to cyclohexane with Ru-NPs produced in **4b**[a]

Catalyst	Conversion[b,c] (%)	Time[d] (min)	TOF[e] (h^{-1})	$TOF_{surface}$[f] (h^{-1})
Ru/**4b**	>99	278	49	122
2nd run	>99	77	218	529
3rd run	>99	75	214	521
4th run	>99	71	256	623
5th run	>99	78	222	542
6th run	97	63	249	606
7th run	>99	61	306	746
8th run	>99	51	312	760
9th run	>99	52	303	738
10th run	97	69	217	529
Ru/**4b**/CS_2[g]	0	240	0	0
Ru/**2b**	33	242	19	64
2nd run	42	241	23	79
3rd run	37	242	18	61

[a] Hydrogenation reaction at 70 °C, 10 bar H_2 using Ru-NPs produced in **4b**. [b] Calculated based on the H_2-consumption. [c] Controlled by headspace GC. [d] Time needed for the given maximum conversion. [e] Turnover frequency = activity as (mol cyclohexane) (mol Ru)$^{-1}$ h^{-1} based on total quantity of Ru present in the nanomaterial. [f] Turnover frequency = activity as (mol cyclohexane) (mol Ru)$^{-1}$ h^{-1} based on the estimated mol (Ru) at the NP surface; see ESI for estimation of surface atoms. [g] CS_2 (0.02 mmol) was dissolved in benzene. The mixture was added to the Ru-NPs before pressurizing the reactor. No conversion could be detected by headspace GC.

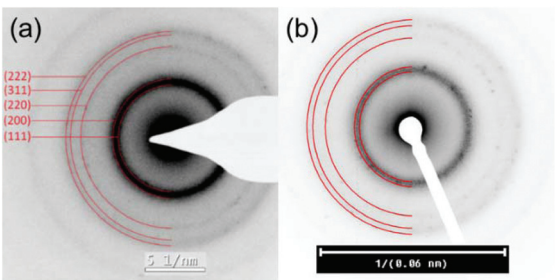

Fig. 9 SAEDs of 1.0 wt% Ru-NPs in **4b** from $Ru_3(CO)_{12}$ before (a) and after catalysis (b) (Ru reference peaks in red from COD 1534914, face centered cubic (fcc) structure with space group $Fm\bar{3}m$).

The catalysis was repeated with the strongly agglomerated Ru-NPs produced in **2b** to compare these results with the separated Ru-NPs produced in **4b** (Table 4, Fig. S53 in the ESI†). The activity of Ru/**2b** was much lower than the activity of Ru/**4b** with a maximal TOF of 79 h^{-1} in the second hydrogenation run. We suggest that the strong aggregation blanks the surface of the Ru-NPs.

As stated in previous works, Ru-NPs can act as reservoirs of active Ru clusters, atoms, or ions, in a mechanism that leaches from the Ru-NPs to act as homogeneous catalysts.[39,72] To test whether the Ru catalyst is homogenous or heterogeneous we added a well-known ruthenium catalyst poison, CS_2. Finke *et al.*[73,74] described this method before. In a heterogeneous catalyst, only a fraction of metal-particle is found on the surface and is catalytically active, so it is possible to poison the catalyst completely with less than 1 equiv. CS_2.[75] For a molecular, homogeneous catalyst ≥1 equiv. CS_2 is needed to poison the catalyst. To poison the catalyst Ru/**4b** 0.41 equiv. CS_2 (corresponding to the surface atoms of Ru/**4b**) were added to the substrate. Even after 4 h, no benzene hydrogenation could be detected (Table 4) which is a strong evidence for a heterogeneous catalyst.

Conclusions

The microwave-assisted thermal decomposition of exemplifying ruthenium and iridium carbonyls indicates a good stabilization of very small M-NPs by TAAILs. The phase purity and absence of carbonyl groups were proven by selected area electron diffraction and attenuated total reflection infrared spectroscopy. Among the different aryl substitution patterns and in comparison to 1-butyl-3-methylimidazolium bis(trifluoromethylsulfonyl)imide (**1**) strong aggregation effects of the primary NPs are evident for **1** and the 2-methylphenyl-substituted ILs (**2**) while the 4-methoxyphenyl- (**3**) and 2,4-dimethylphenyl-substituted ILs (**4**) lead to well separated particles. This aggregation difference could be traced to the differences in the electron density of the substituents on the phenyl group, such that the 4-methoxy and 4-methyl groups assume a higher negative electrostatic potential. The 2-methyl substituent on the phenyl ring in **2** (and **4**) and also the 3-methyl group on the imidazolium core in **1** possesses less electron density. This work shows that the implementation of an electron donating *para*-substituent on the phenyl ring in the phenylimidazolium cation is an easy measure to achieve well-separated M-NPs if aggregation is a problem and is desired to be avoided.

Aggregation effects induced by interactions of the washing agents with the ILs in the TEM preparation could be ruled out by ε-ePC-SAFT modelling of activity coefficients and IL solubility in the solvents.

Separated Ru-NPs produced in **4b** were re-usable catalysts for the hydrogenation of benzene. The hydrogenation was successful with turnover frequencies up to 760 h^{-1} over ten catalysis runs, whereas agglomerated Ru-NPs produced in **2b** show low activity up to 79 h^{-1}. Further investigation can focus on supplemental separation of high agglomerated M-NPs like magnetic cobalt or iron nanoparticles.

Conflicts of interest

There are no conflicts to declare.

Acknowledgements

This work has been supported by the German Science Foundation (DFG) within the priority program SPP 1708 "*Material Synthesis Near Room Temperature*" (grant STR 526/20-1/2 for TS, grant HE 7165/7-1 for CH and grant JA 466/31-1/2 for CJ). We acknowledge the Ernst Ruska-Centre (Forschungszentrum Jülich GmbH, Jülich, Germany) and

Dr Juri Barthel for access to the TEM facility and technical support under project number ER-C A-060. We thank Mr Volker Kree (Max-Planck-Institut für Eisenforschung GmbH, Düsseldorf, Germany) for part of the TEM and SAED measurements.

Notes and references

1 M. Bruchez, M. Moronne, P. Gin, S. Weiss and A. P. Alivisatos, *Science*, 1998, **281**, 2013–2016.
2 K. Saha, S. S. Agasti, C. Kim, X. Li and V. M. Rotello, *Chem. Rev.*, 2012, **112**, 2739–2779.
3 J. H. Li and J. Z. Zhang, *Coord. Chem. Rev.*, 2009, **253**, 3015–3041.
4 W. L. Barnes, A. Dereux and T. W. Ebbesen, *Nature*, 2003, **424**, 824–830.
5 P. Poizot, S. Laruelle, S. Grugeon, L. Dupont and J. M. Tarascon, *Nature*, 2000, **407**, 496–499.
6 L. Armelao, S. Quici, F. Barigelletti, G. Accorsi, G. Bottaro, M. Cavazzini and E. Tondello, *Coord. Chem. Rev.*, 2010, **254**, 487–505.
7 J. D. Scholten, B. C. Leal and J. Dupont, *ACS Catal.*, 2012, **2**, 184–200.
8 D. Astruc, F. Lu and J. R. Aranzaes, *Angew. Chem., Int. Ed.*, 2005, **44**, 7852–7872.
9 P. Zhao, X. Feng, D. Huang, G. Yang and D. Astruc, *Coord. Chem. Rev.*, 2015, **287**, 114–136.
10 J. M. Walker and J. M. Zaleski, *Nanoscale*, 2016, **8**, 1535–1544.
11 A. Gual, C. Godard, S. Castillón and C. Claver, *Dalton Trans.*, 2010, **39**, 11499–11512.
12 J. Aguilera, I. Favier, M. Sans, A. Mor, A. Álvarez-Larena, O. Illa, M. Gómez and R. M. Ortuño, *Eur. J. Org. Chem.*, 2015, 810–819.
13 Y. Huang, Y. Mao, Y. Cheng, L. Wang and X. Li, *Appl. Catal., A*, 2015, **495**, 124–130.
14 L. Foppa, L. Luza, A. Gua, D. E. Weibel, D. Eberhardt, S. R. Texeira and J. Dupont, *Dalton Trans.*, 2015, **44**, 2827–2834.
15 D. Marquardt, C. Vollmer, R. Thomann, P. Steurer, R. Mülhaupt, E. Redel and C. Janiak, *Carbon*, 2011, **49**, 1326–1332.
16 R. Marcos Esteban, K. Schütte, D. Marquardt, J. Barthel, F. Beckert, R. Müllhaupt and C. Janiak, *Nano-Struct. Nano-Objects*, 2015, **2**, 28–34.
17 S. Wegner, C. Rutz, K. Schütte, J. Barthel, A. Bushmelev, A. Schmidt, K. Dilchert, R. A. Fischer and C. Janiak, *Chem. – Eur. J.*, 2017, **23**, 6330–6340.
18 W. Ostwald, *Z. Phys. Chem.*, 1901, **37**, 385.
19 W. Ostwald, *Lehrbuch der Allgemeinen Chemie*, Engelmann, Leipzig, 1896.
20 C. Janiak, *Z. Naturforsch., B: J. Chem. Sci.*, 2013, **68**, 1059–1089.
21 C. Vollmer and C. Janiak, *Coord. Chem. Rev.*, 2011, **255**, 2039–2057.
22 P. S. Campbell, M. H. G. Prechtl, C. C. Santini and P.-H. Haumesser, *Curr. Org. Chem.*, 2013, **17**, 414–429.
23 D. Freudenmann, S. Wolf, M. Wolff and C. Feldmann, *Angew. Chem., Int. Ed.*, 2011, **50**, 11050–11060.
24 E. Ahmed, J. Breternitz, M. F. Groh and M. Ruck, *CrystEngComm*, 2012, **14**, 4874–4885.
25 H. Kaper, F. Endres, I. Djerdj, M. Antonietti, B. M. Smarsly, J. Maier and Y.-S. Hu, *Small*, 2007, **3**, 1753–1763.
26 M. Antonietti, D. Kuang, B. Smarsly and Y. Zhou, *Angew. Chem., Int. Ed.*, 2004, **43**, 4988–4922.
27 D. Marquardt and C. Janiak, *Nachr. Chem.*, 2013, **61**, 754–757.
28 J. Dupont and J. D. Scholten, *Chem. Soc. Rev.*, 2010, **39**, 1780–1804.
29 P. Wasserscheid and W. Keim, *Angew. Chem., Int. Ed.*, 2000, **39**, 3772–3789.
30 J. Dupont, *J. Braz. Chem. Soc.*, 2004, **15**, 341–350.
31 E. Redel, M. Walter, R. Thomann, C. Vollmer, L. Hussein, H. Scherer, M. Krüger and C. Janiak, *Chem. – Eur. J.*, 2009, **15**, 10047–10059.
32 E. Redel, R. Thomann and C. Janiak, *Chem. Commun.*, 2008, 1789–1791.
33 E. Redel, R. Thomann and C. Janiak, *Inorg. Chem.*, 2008, **47**, 14–16.
34 T. Strassner and S. Ahrens, *EP* 2254871B1, 2008.
35 S. Ahrens, A. Peritz and T. Strassner, *Angew. Chem., Int. Ed.*, 2009, **48**, 7908–7910.
36 T. Strassner, T. Schulz, G. Bernhard, J. Raff and F. Lehmann, *EP* 2739572B1, 2013.
37 F. Schroeter, S. Lerch, M. Kaliner and T. Strassner, *Org. Lett.*, 2018, **20**, 6215–6219.
38 C. Vollmer, R. Thomann and C. Janiak, *Dalton Trans.*, 2012, **41**, 9722–9727.
39 C. Vollmer, E. Redel, K. Abu-Shandi, R. Thomann, H. Manyar, C. Hardacre and C. Janiak, *Chem. – Eur. J.*, 2010, **16**, 3849–3858.
40 T. Gutel, J. Garcia-Anton, K. Pelzer, K. Philippot, C. C. Santini, Y. Chauvin, B. Chaudret and J.-M. Basset, *J. Mater. Chem.*, 2007, **17**, 3290–3292.
41 E. T. Silveira, A. P. Umpierre, L. M. Rossi, G. Machado, J. Morais, G. V. Soares, I. J. R. Baumvol, S. R. Teixeira, R. F. P. Fichtner and J. Dupont, *Chem. – Eur. J.*, 2004, **10**, 3734–3740.
42 K. Pelzer, O. Vidoni, K. Philippot, B. Chaudret and V. Collière, *Adv. Funct. Mater.*, 2003, **13**, 118–126.
43 J. Krämer, E. Redel, R. Thomann and C. Janiak, *Organometallics*, 2008, **27**, 1976–1978.
44 E. Redel, J. Krämer, R. Thomann and C. Janiak, *J. Organomet. Chem.*, 2009, **694**, 1069–1075.
45 G. S. Fonseca, G. Machado, S. R. Teixeira, G. H. Fecher, J. Morais, M. C. M. Alves and J. Dupont, *J. Colloid Interface Sci.*, 2006, **301**, 193–204.
46 M. J. Frisch, G. W. Trucks, H. B. Schlegel, G. E. Scuseria, M. A. Robb, J. R. Cheeseman, G. Scalmani, V. Barone, G. A. Petersson, H. Nakatsuji, X. Li, M. Caricato, A. V. Marenich, J. Bloino, B. G. Janesko, R. Gomperts, B. Mennucci, H. P. Hratchian, J. V. Ortiz, A. F. Izmaylov,

J. L. Sonnenberg, D. Williams-Young, F. Ding, F. Lipparini, F. Egidi, J. Goings, B. Peng, A. Petrone, T. Henderson, D. Ranasinghe, V. G. Zakrzewski, J. Gao, N. Rega, G. Zheng, W. Liang, M. Hada, M. Ehara, K. Toyota, R. Fukuda, J. Hasegawa, M. Ishida, T. Nakajima, Y. Honda, O. Kitao, H. Nakai, T. Vreven, K. Throssell, J. A. Montgomery Jr., J. E. Peralta, F. Ogliaro, M. J. Bearpark, J. J. Heyd, E. N. Brothers, K. N. Kudin, V. N. Staroverov, T. A. Keith, R. Kobayashi, J. Normand, K. Raghavachari, A. P. Rendell, J. C. Burant, S. S. Iyengar, J. Tomasi, M. Cossi, J. M. Millam, M. Klene, C. Adamo, R. Cammi, J. W. Ochterski, R. L. Martin, K. Morokuma, O. Farkas, J. B. Foresman and D. J. Fox, *Gaussian 16, Revision A.03*, Gaussian, Inc., Wallingford CT, 2016.

47 A. D. Becke, *J. Chem. Phys.*, 1993, **98**, 5648–5652.

48 C. Lee, W. Yang and R. G. Parr, *Phys. Rev. B: Condens. Matter Mater. Phys.*, 1988, **37**, 785–789.

49 P. Stephens, F. J. Devlin, C. F. Chabalowski and M. J. Frisch, *J. Phys. Chem.*, 1994, **98**, 11623–11627.

50 S. H. Vosko, L. Wilk and M. Nusair, *Can. J. Phys.*, 1980, **58**, 1200–1211.

51 R. Dennington, T. A. Keith and J. M. Millam, *GaussView, Version 6*, Semichem Inc., Shawnee Mission, KS, 2016.

52 C. Rutz, L. Schmolke, V. Gvilava and C. Janiak, *Z. Anorg. Allg. Chem.*, 2017, **643**, 130–135.

53 M. Larhed, C. Moberg and A. Hallberg, *Acc. Chem. Res.*, 2002, **35**, 717–727.

54 E. Redel, M. Walter, R. Thomann, L. Hussein, M. Krüger and C. Janiak, *Chem. Commun.*, 2010, **46**, 1159–1161.

55 M. Yang, P. S. Campbell, C. C. Santini and A. V. Mudring, *Nanoscale*, 2014, **6**, 3367–3375.

56 Y. Hatakeyama, M. Okamoto, T. Torimoto, S. Kuwabata and K. Nishikawa, *J. Phys. Chem. C*, 2009, **113**, 3917–3922.

57 P. Migowski, G. Machado, S. R. Texeira, M. C. M. Alves, J. Morais, A. Traverse and J. Dupont, *Phys. Chem. Chem. Phys.*, 2007, **9**, 4814–4821.

58 A. Podgorsek, A. Pensado, C. Santini, M. Gomes and A. Padua, *J. Phys. Chem. C*, 2013, **117**, 3537–3547.

59 M. Bülow, X. Ji and C. Held, *Fluid Phase Equilib.*, 2019, submitted.

60 K. Klauke, D. H. Zaitsau, M. Bülow, L. He, M. Klopotowski, T.-O. Knedel, J. Barthel, C. Held, S. P. Verevkin and C. Janiak, *Dalton Trans.*, 2018, **47**, 5083–5097.

61 X. Ji, C. Held and G. Sadowski, *Fluid Phase Equilib.*, 2012, **335**, 64–73.

62 X. Ji, C. Held and G. Sadowski, *Fluid Phase Equilib.*, 2014, **363**, 59–65.

63 C. Held, T. Reschke, S. Mohammad, A. Luza and G. Sadowski, *Chem. Eng. Res. Des.*, 2014, **92**, 2884–2897.

64 H. Bi, X. Tan, R. Dou, Y. Pei, M. Qiao, B. Sun and B. Zong, *Green Chem.*, 2016, **18**, 2216–2221.

65 Y. Wan, C. Chen, W. Xiao, L. Jian and N. Zhang, *Microporous Mesoporous Mater.*, 2013, **171**, 9–13.

66 K. B. Sidhpuria, H. A. Patel, P. A. Parikh, P. Bahadur, H. C. Bajaj and R. V. Jasra, *Appl. Clay Sci.*, 2009, **42**, 386–390.

67 E. T. Silveira, A. P. Umpierre, L. M. Rossi, G. Machado, J. Morais, G. V. Soares, I. J. R. Baumvol, S. R. Teixeira, P. F. P. Fichtner and J. Dupont, *Chem. – Eur. J.*, 2004, **10**, 3734–3740.

68 S. K. Sharma, K. B. Sidhpuria and R. V. Jasra, *J. Mol. Catal. A: Chem.*, 2011, **335**, 65–70.

69 A. Stanislaus and B. H. Cooper, *Catal. Rev. Sci. Eng.*, 1994, **36**, 75–123.

70 K. Weissermel and H.-J. Arpe, *Industrial Organic Chemistry*, Wiley-VCH, Weinheim, 2003.

71 J.-F. Le Page, *Applied Heterogeneous Catalysis: Design, Manufacture, Use of Solid Catalysts*, Technip, Paris, 1987.

72 L. Durán Pachón and G. Rothenberg, *Appl. Organomet. Chem.*, 2008, **22**, 288–299.

73 B. J. Hornstein, J. D. Aikon III and R. G. Finke, *Inorg. Chem.*, 2002, **41**, 1625–1638.

74 Y. Lin and R. G. Finke, *Inorg. Chem.*, 1994, **33**, 4891–4910.

75 J. A. Widegren, M. A. Bennett and R. G. Finke, *J. Am. Chem. Soc.*, 2003, **125**, 10301–10310.